scientific reports

Check for updates

OPEN

β-Nicotinamide mononucleotide preserves muscle strength in septic male mice

Mari Saida[1,2], Noritaka Saeki[3,4,5], Hiroshi Sakai[4,6], Jun Iwanami[7], Atsushi Yokoyama[8], Shun Sawatsubashi[9], Motoi Kanagawa[7], Norio Sato[1] & Yuuki Imai[4,6]✉

Sepsis remains a leading cause of mortality and long-term disability, with survivors frequently developing intensive care unit–acquired weakness (ICU-AW) as part of post-intensive care syndrome. To identify a nutritional therapy for ICU-AW, we investigated the mechanisms underlying sepsis-induced skeletal muscle dysfunction using a cecal slurry-induced sepsis mouse model. Although body weight and skeletal muscle mass recovered 14 days after sepsis induction, muscle strength remained impaired, accompanied by persistent mitochondrial abnormalities. Transcriptomic analysis revealed that the pathways termed the 'sirtuin signaling pathway' and 'mitochondrial dysfunction' significantly enriched and *Sirt3*, a major mitochondrial nicotinamide adenine dinucleotide (NAD^+)-dependent deacetylase, was downregulated. Biochemical analyses confirmed increased acetylated lysine of mitochondrial proteins in septic muscle tissue. Among these proteins, mass spectrometry detected several proteins in the acetylated band, including multiple complex I subunits. Whether these are direct SIRT3 targets remains to be determined. Knockdown of *Sirt3* in C2C12 myotubes impaired mitochondrial respiration, whereas treatment with β-nicotinamide mononucleotide (β-NMN) partially rescued energy production. *In vivo*, acute-phase administration of β-NMN preserved mitochondrial morphology and skeletal muscle strength without altering muscle mass. These findings demonstrate that sepsis induces mitochondrial dysfunction and persistent muscle weakness associated with Sirt3 downregulation, and highlights β-NMN supplementation as a promising NAD^+-targeted therapeutic strategy for mitigating ICU-AW.

Keywords β-NMN, Mitochondrial respiration, Sirt3, Skeletal muscle weakness, Sepsis

Sepsis is defined as life-threatening organ dysfunction caused by a dysregulated host response to infection. It remains a leading cause of death and disability worldwide[1]. While advances in intensive care medicine have improved short-term survival for sepsis patients, many survivors subsequently develop long-lasting sequelae known as post-intensive care syndrome (PICS)[2]. A key component of PICS is intensive care unit-acquired weakness (ICU-AW), which is characterized by diffuse skeletal muscle weakness in seriously ill patients without specific causes other than the critical illness itself[3,4]. Skeletal muscle atrophy frequently develops early during critical illness and contributes to ICU-AW. It has been suggested that approximately 25–80% of ICU survivors are afflicted with ICU-AW, although the incidence varies depending on patient characteristics[4–6]. This muscle weakness is associated with prolonged ventilation, extended ICU stays, and increased mortality as well as a decline in quality of life after ICU discharge[7].

Recovery from pathological loss of skeletal muscle mass does not necessarily result in restoration of muscle strength. Previous studies have reported that even when skeletal muscle mass returns to normal after recovery from sepsis, muscle strength often remains impaired for prolonged periods[8,9]. These observations suggest that

[1]Department of Emergency and Critical Care Medicine, Ehime University Graduate School of Medicine, Toon, Ehime, Japan. [2]Department of Clinical Nutrition and Food Management, Saiseikai Yokohamashi Tobu Hospital, Yokohama, Kanagawa, Japan. [3]Division of Research Coordination and Technical Development Office, PIAS, Ehime University, Matsuyama, Ehime, Japan. [4]Division of Integrative Pathophysiology, Proteo-Science Center, PIAS, Ehime University, Toon, Ehime, Japan. [5]Department of Applied Chemistry, Ehime University Graduate School of Science and Engineering, Matsuyama, Ehime, Japan. [6]Department of Pathophysiology, Ehime University Graduate School of Medicine, Toon, Ehime, Japan. [7]Department of Cell Biology and Molecular Medicine, Ehime University Graduate School of Medicine, Toon, Ehime, Japan. [8]Department of Molecular Endocrinology, Tohoku University Graduate School of Medicine, Sendai Miyagi, Japan. [9]Research and Innovation Liaison Office, Institute of Advanced Medical Sciences, Tokushima University, Tokushima, Tokushima, Japan. ✉email: y-imai@m.ehime-u.ac.jp

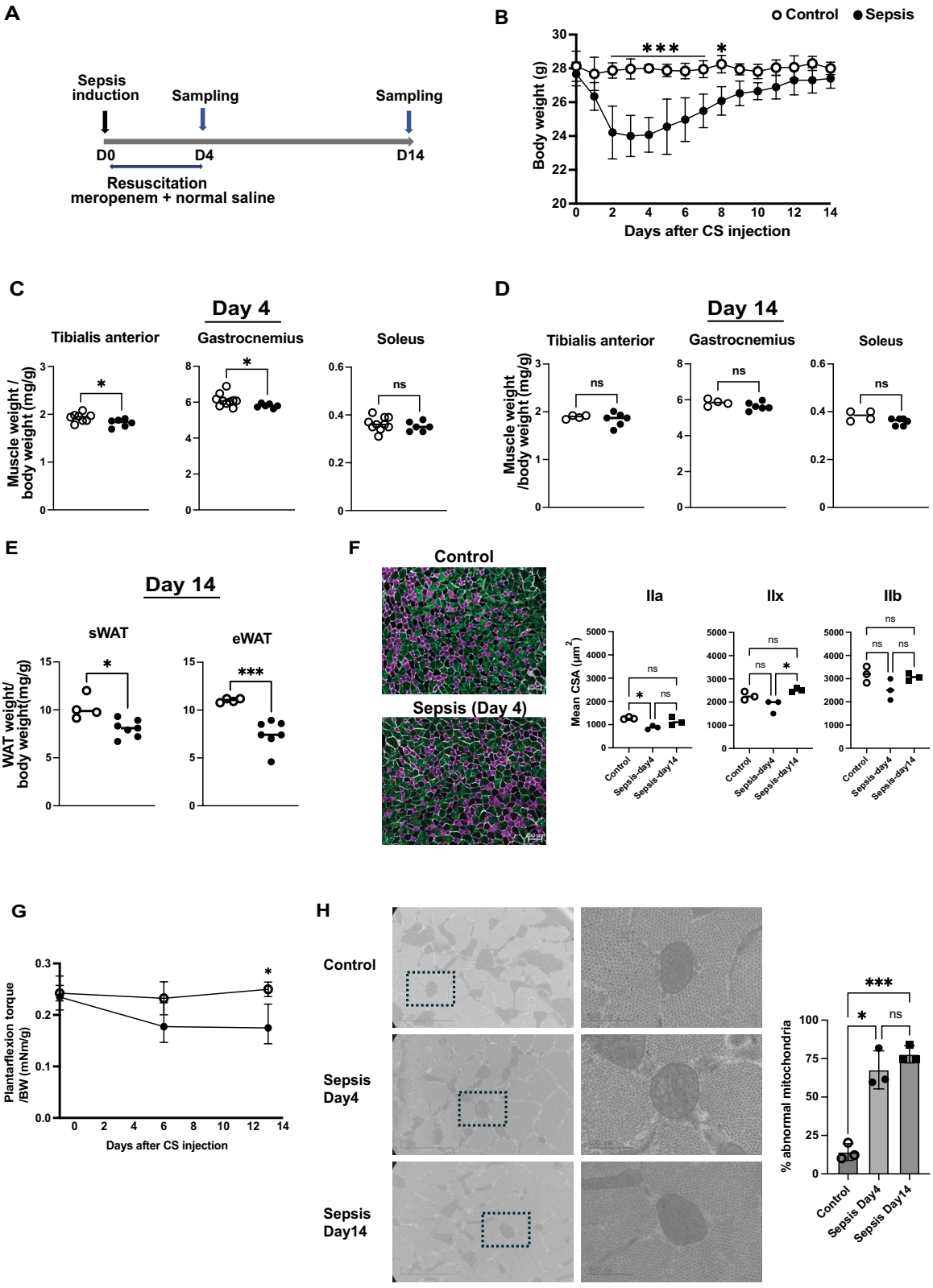

factors beyond muscle atrophy, such as deterioration of muscle quality, contribute to persistent post-sepsis muscle weakness. Recent studies have demonstrated chronic muscle weakness associated with mitochondrial abnormalities, despite the absence of sustained muscle atrophy, using a sepsis mouse model, supporting the notion that mitochondrial dysfunction may underlie ICU-AW[8,10].

Nutritional therapy is an essential component of critical care management. In the ICU, energy and protein delivery are generally adjusted according to the patient's condition, with increasing emphasis on individualized approaches[11,12], although such individualized nutritional management remains unclear. Moreover, specific nutritional strategies aimed at preventing sepsis-induced muscle weakness have not been established. While

◀**Fig. 1**. Skeletal muscle function remained impaired after morphological recovery in sepsis model. (**A**) Experimental timeline of the cecal slurry (CS)-induced sepsis model in 11–13-week-old mice. Sepsis was induced at day 0 (D0), and mice were resuscitated with meropenem and normal saline. Muscle tissues were harvested at D4 and D14. (**B**) Body weight changes after CS injection (control = open circles; sepsis group = filled circle; control, n = 4; sepsis, n = 6). (**C**, **D**) Muscle weights of the tibialis anterior, gastrocnemius, and soleus muscles at D4 (**C**) and D14 (**D**) after CS injection (D4: control, n = 10; sepsis, n = 6; D14: control, n = 4; sepsis, n = 6). (**E**) Weights of subcutaneous and epididymal white adipose tissue (sWAT and eWAT, respectively) depots at D14 for mice with sepsis. (**F**) Representative immunofluorescence images of gastrocnemius muscle fiber cross-sections. Laminin (white), type IIa fibers (magenta), and type IIb fibers (green) were stained, while type IIx fibers remained unstained and appear black. Quantification of cross-sectional area by fiber type is shown on the right (n = 3 per group). Scale bar = 100 µm. (**G**) Ratio of plantar flexor torque to body weight, measured at one day before sepsis induction (baseline), and on days 6 and 13 after sepsis induction in the same mice (control, n = 4; sepsis, n = 6). (**H**) Representative transmission electron microscopy images of the gastrocnemius muscle in control and septic mice at days 4 and 14 after CS injection (n = 3 per group). The boxed areas in the left panels are shown at higher magnification in the right panels. Scale bars: 2 µm (left panels) and 500 nm (right panels). Data are presented as mean ± SEM. Muscle torque data (**G**) were analyzed by two-way repeated measures ANOVA to test the effects of group (control vs sepsis) at each time point (D6 and D13), followed by post-hoc multiple comparisons with Bonferroni correction. Skeletal muscle weight and WAT data (**C**, **D**, **E**) were analyzed using unpaired Welch's *t*-test. $^{*}p < 0.05$, $^{***}p < 0.001$, ns, not significant.

early mobilization and general nutritional support have shown partial benefits in mitigating ICU-AW[13,14], interventions targeting cellular metabolism remain poorly investigated in the acute phase of sepsis.

In this study, we aimed to explore the potential of acute-phase nutritional therapy to preserve muscle function using a mouse model. Our transcriptome analysis revealed that mRNA levels of *Sirt3* decreased in septic skeletal muscle. SIRT3 is a major mitochondrial NAD^+-dependent deacetylase that regulates the acetylation status of respiratory chain proteins and maintains mitochondrial oxidative phosphorylation[15]. Reduced SIRT3 activity can lead to hyperacetylation of mitochondrial proteins, impaired complex activity, and decreased ATP production[15]. Our data show that the acetylation of complex I -associated proteins is increased in septic skeletal muscle, and mitochondrial respiration is impaired in *Sirt3*-knockdown C2C12 cells. Furthermore, acute-phase administration of nicotinamide mononucleotide (NMN), a precursor of NAD^+, appeared to attenuate muscle weakness and partially restore mitochondrial function, suggesting a potential therapeutic role for NAD^+ repletion in the prevention of sepsis-induced muscle dysfunction.

Results

Skeletal muscle function remained impaired after morphological recovery in a sepsis mouse model

To examine the effects of sepsis on skeletal muscle, we generated a cecal slurry (CS)-inducible sepsis animal model using young mice based on a previous report[16]. Therapeutic intervention with an antibiotic was conducted for 5 days after CS injection (Fig. 1A). To validate sepsis pathogenesis in the model, we assessed survival rate, body temperature, inflammatory cytokine level, and histological evidence of organ dysfunction. Overall survival rate was 50% in the sepsis model (Fig. S1A). Body temperature reached its lowest point 12 h after CS injection, then gradually increased and returned to baseline by day 4 (Fig. S1B), which was broadly consistent with previous reports using the CS-induced sepsis model[16]. On day 4 after CS administration, serum IL-6 an inflammatory cytokine, was significantly elevated in septic mice (Fig. S1C). Histological analysis demonstrated tubular swelling, vacuolar degeneration of renal tubular epithelium, and luminal dilatation in the kidney, together with pronounced thickening of the alveolar walls in the lung, consistent with multiple organ failure (Fig. S1D). These results indicate that CS administration in mice successfully reproduced septic pathology. Next, we assessed changes in body weight and skeletal muscle mass, and we measured muscle strength following sepsis induction. Body weight drastically declined until days 3–4 after sepsis induction, and then gradually recovered and returned toward baseline by days 12–14 (Fig. 1B). On day 4 after sepsis induction, the skeletal muscle weights of that predominantly contain fast-twitch muscle fibers, including tibialis anterior and gastrocnemius, were significantly reduced in septic mice compared with controls. In contrast, no significant difference was observed in the weights of soleus, that predominantly contains slow-twitch muscle fibers (Fig. 1C). By day 14, the skeletal muscle weights had largely recovered, showing no significant difference between the sepsis and control group (Fig. 1D). Conversely, the weights of epididymal and subcutaneous white adipose tissue (eWAT and sWAT, respectively) remained significantly decreased on day 14, indicating a persistent loss of adipose tissue despite recovery of body weight (Fig. 1E). Histological analysis of gastrocnemius muscles on day 14 revealed that the cross-sectional area (CSA) of myofibers had returned to near-control levels, consistent with the recovery of skeletal muscle mass (Fig. 1F). However, the plantarflexion force of the ankle joint remained significantly reduced on both days 6 and 13 after sepsis induction despite the recovery of skeletal muscle weight (Fig. 1G). Mitochondria are essential regulators of skeletal muscle energy metabolism and have been implicated in the pathophysiology of sepsis-induced muscle dysfunction[8,17,18]. Transmission electron microscopy (TEM) revealed morphological abnormalities of mitochondria in gastrocnemius muscles of septic mice on both days 4 and 14, including disrupted and fragmented cristae, and reduced matrix electron density (Fig. 1H). These ultrastructural changes were already evident on day 4 but became more pronounced by day 14, indicating that mitochondrial damage persisted and even progressed despite recovery of muscle mass and morphology. These

findings are consistent with previous reports using aged septic mice[8], and persistent muscle weakness after sepsis was exhibited, even in young mice. Such ultrastructural abnormalities suggest impaired mitochondrial quality control. This impairment likely underlies the prolonged deficit in skeletal muscle contractile function observed after sepsis, despite recovery of muscle mass and morphology, and thus reflects key features of ICU-AW.

Identification of sepsis-induced gene expression changes in skeletal muscle

To investigate the molecular mechanisms underlying the persistent muscle weakness observed to be associated with sepsis, we performed RNA sequencing (RNA-seq) using mRNA obtained from gastrocnemius muscle tissue in septic mice on day 4 after sepsis induction and from control mice. Principal component analysis (PCA) revealed distinct gene expression profiles between the groups, indicating that sepsis induced substantial transcriptomic alterations (Fig. 2A). Hierarchical clustering analysis also revealed distinct clustering between the septic and control groups (Fig. 2B). In total, 1016 genes were significantly upregulated, and 933 genes were significantly downregulated in septic mice compared with controls (Fig. 2C). To explore the biological pathways associated with these changes in gene expression, we performed Ingenuity Pathway Analysis (IPA) using the entire set of differentially expressed genes. This analysis revealed that pathways related to mitochondrial metabolism and cellular energy homeostasis, including sirtuin signaling, mitochondrial dysfunction, and oxidative phosphorylation, were significantly enriched among the top 5 enriched canonical pathways (Fig. 2D). Sirtuins are class III histone deacetylases that utilize NAD^+ as a co-substrate, and are known to regulate cellular metabolism, stress responses, and aging[19,20]. To confirm the sirtuin family expression, we assessed the mRNA expression levels of all seven sirtuin family members (*Sirt1* to *Sirt7*) in the gastrocnemius muscle using real-time (RT)-qPCR. Among them, *Sirt3, Sirt4, Sirt5*, and *Sirt6* were significantly downregulated in the sepsis group, while *Sirt2* was slightly upregulated. No significant changes were observed in *Sirt1* and *Sirt7* (Fig. 2E). Notably, SIRT3, SIRT4, and SIRT5, which are localized in mitochondria, were significantly downregulated in the septic group, suggesting a potential link between mitochondrial sirtuin suppression and sepsis-induced mitochondrial dysfunction. We focused on SIRT3 because it is recognized as the primary mitochondrial deacetylase that broadly regulates the acetylation status of mitochondrial proteins and thereby exerts central control over mitochondrial metabolism and function[21]. Consistent with a previous report[22], IPA also predicted that various molecules in these pathways could be influenced by downregulation of *Sirt3* (Fig. S2). Collectively, our transcriptomic and subsequent pathway analyses revealed that sepsis induced significant gene expression changes particularly affecting pathways associated with mitochondrial function and energy metabolism in skeletal muscle and suggested that *Sirt3* is one of the key regulators of mitochondrial dysfunction in sepsis.

Impaired respiration associated with Sirt3 knockdown is partially rescued by *β*-NMN treatment in C2C12

To investigate whether protein acetylation is altered in skeletal muscle mitochondria during sepsis, we first performed Western blotting for acetyl-lysine in mitochondria lysate isolated from gastrocnemius muscles on day 4 after sepsis induction. The signal intensity of acetyl-lysine was markedly increased in septic mice, particularly of approximate molecular weight 20 kDa, suggesting insufficient deacetylation by downregulated deacetylases including *Sirt3* during the acute phase of sepsis (Fig. 3A). Mass spectrometry analysis using proteins of approximately 20 kDa in sepsis revealed several candidate substrate proteins of *Sirt3*, among which multiple subunits of mitochondrial complex I were highly enriched (Fig. 3B). Of the top 10 candidates identified, several subunits of mitochondrial respiratory complex I were present, suggesting that abnormal acetylation of complex I may be associated with mitochondrial dysfunction in skeletal muscle during sepsis.

To further investigate the pathophysiological significance of the decreased *Sirt3* expression observed in the muscle of septic mice, we established an in vitro model by knocking down *Sirt3* in C2C12 myotubes using small interfering RNA (siRNA) (Fig. 3C, D and E). To evaluate the functional consequences of *Sirt3* depletion, we performed a mitochondrial stress test using a flux analyzer. Knockdown of *Sirt3* in C2C12 myotubes resulted in a marked reduction in basal and maximal respiration, ATP production, and proton leak, indicating impaired mitochondrial respiratory capacity (Fig. 3F). Given that sirtuin activity is dependent on NAD^+ availability, we hypothesized that NAD^+ precursor supplementation might restore sirtuin function and ameliorate mitochondrial dysfunction in myotubes with experimentally reduced Sirt3 expression, mimicking the decrease in *Sirt3* observed during sepsis. To examine whether supplementation with an NAD^+ precursor alters intracellular NAD^+ levels and mitochondrial function, C2C12 myotubes with *Sirt3* knockdown were treated with β-NMN (Fig. 3G). Knockdown of *Sirt3* in C2C12 myotubes significantly reduced intracellular NAD^+ levels, whereas β-NMN treatment significantly and partially increased intracellular NAD^+ levels (Fig. 3H). Therefore, treatment with *β*-NMN, a key NAD^+ precursor, selectively improved basal respiration and ATP production, whereas maximal respiration and proton leak remained suppressed (Fig. 3I). These findings suggest that NAD^+ supplementation can partially rescue mitochondrial dysfunction associated with reduced SIRT3 activity in vitro, particularly in supporting energy production.

β-NMN prevented functional decline in skeletal muscle after sepsis

To assess the effects of *β*-NMN *in vivo*, mice with sepsis were treated with *β*-NMN every third day from days 3 to 12 after sepsis induction and their body weight, skeletal muscle mass, WAT mass, and muscle strength were measured (Fig. 4A). Survival rates did not differ between the Sepsis-PBS and Sepsis–*β*-NMN groups (Fig. S3A). There were no significant differences in the change in body weights over 14 days with or without *β*-NMN treatment (Fig. 4B). Similarly, skeletal muscle mass (of the tibialis anterior, gastrocnemius, and soleus) as well as sWAT and eWAT were comparable between the groups (Fig. 4C and D). Conversely, muscle strength, assessed using electrical stimulation plantarflexion torque, was significantly higher in the *β*-NMN-treated group than that in the Sepsis-PBS group at day 13 (Fig. 4E). Within-group comparisons revealed that muscle strength

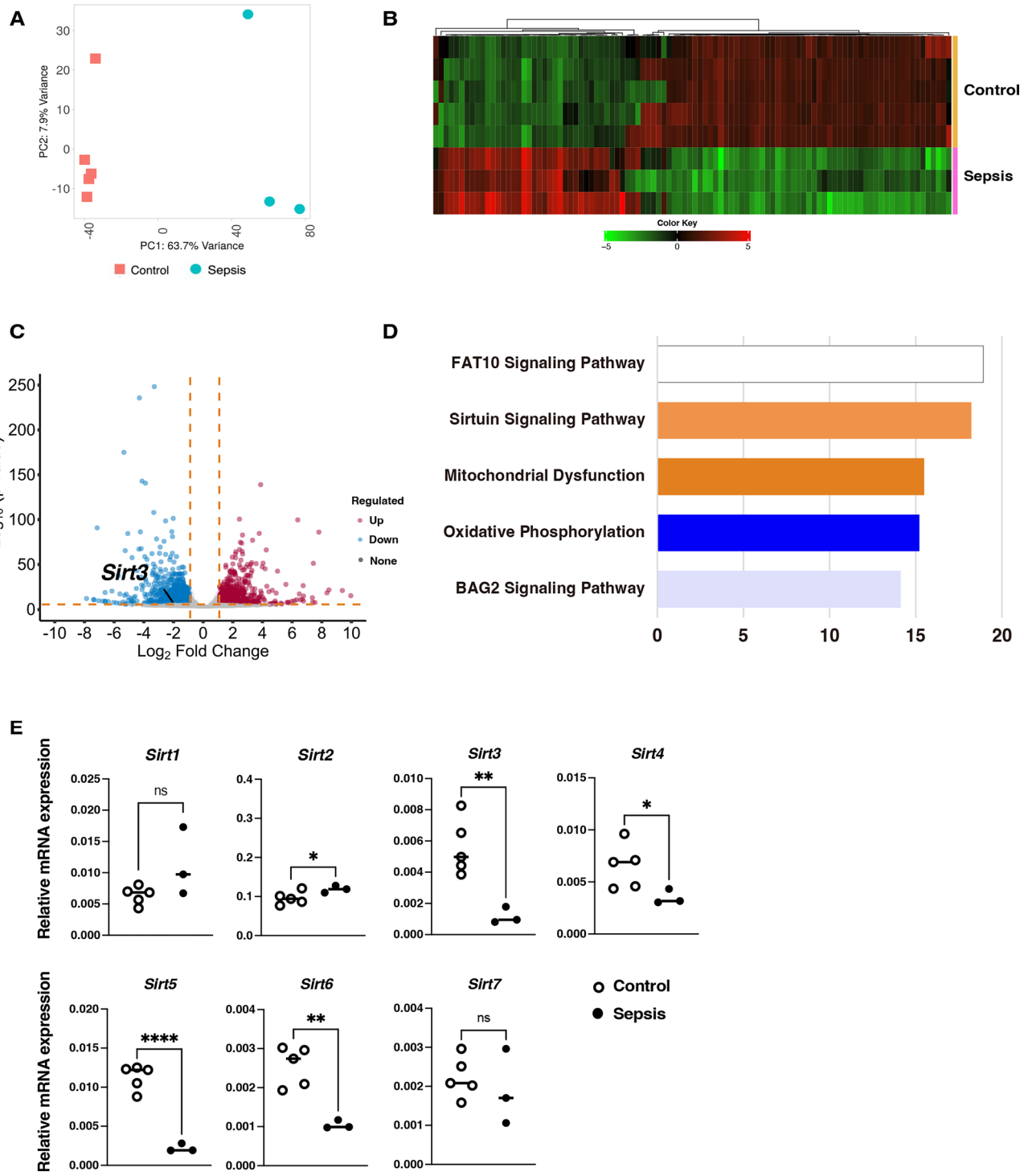

Fig. 2. Identification of sepsis-induced gene expression changes in skeletal muscle. (**A**) Principal component analysis (PCA) of RNA-seq showing the separation of control and sepsis groups based on transcriptomic profiles of gastrocnemius muscle at day 4 after cecal slurry injection. (**B**) Heatmap of representative differentially expressed genes (DEGs) between control and sepsis groups on day 4. (**C**) Volcano plot displaying DEGs in gastrocnemius muscle on day 4 after CS injection. (**D**) Canonical pathway analysis of DEGs using Ingenuity Pathway Analysis (IPA). The top five enriched pathways are shown, including those related to mitochondrial function and sirtuin signaling. (**E**) Quantitative PCR analysis of the sirtuin family genes (*Sirt1–7*) in the gastrocnemius muscle at day 4 after sepsis induction. All analyses were performed using the same set of samples (control, n = 5; sepsis, n = 3). Data are presented as mean ± SEM. Statistical significance of qPCR results (**E**) was determined using unpaired Welch's *t*-test between control and sepsis groups. $^{*}p < 0.05$, $^{**}p < 0.01$, $^{****}p < 0.0001$; ns, not significant.

B

Gene symbol	Mascot score	# peptides	# unique peptides	MW [kDa]	Abundance (scaled)
Ndufb7	4292	5	5	16.3	100
Ndufb6	3787	8	8	15.5	100.03
Ndufa12	2917	5	5	17.1	100
Cox4i1	2659	6	6	19.5	99.97
Ndufa13	1853	5	5	16.8	100
Mgst3	1758	4	4	16.9	99.97
Coq7	1502	8	8	24	100
Atp5f1d	1159	3	3	17.6	100
Ndufa8	1158	4	4	20	100.03
Apoo	1117	4	4	22.6	99.97

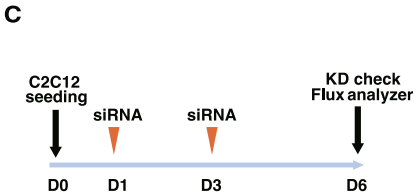

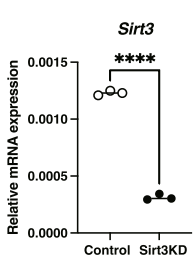

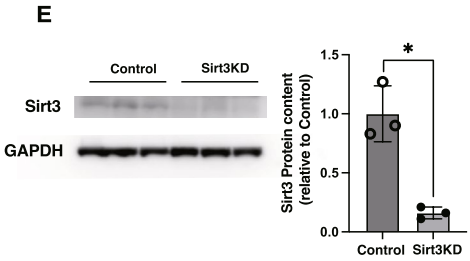

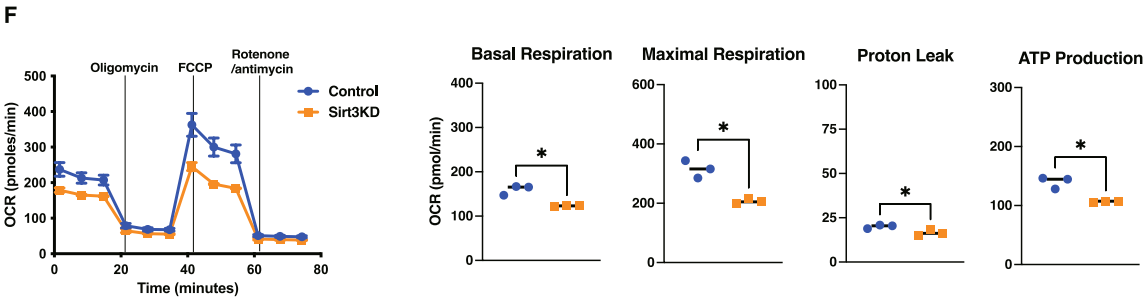

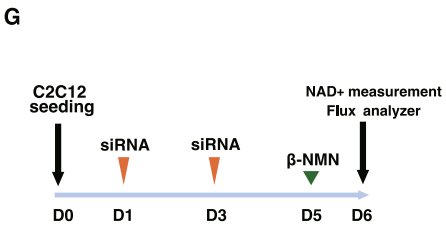

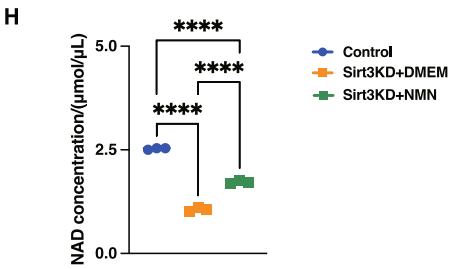

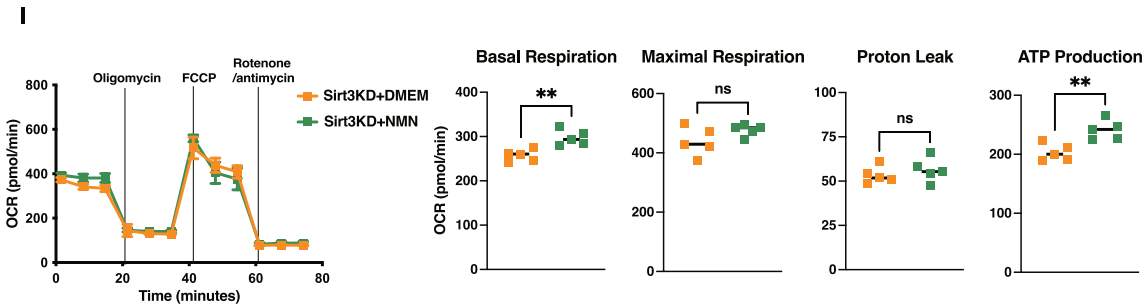

significantly declined from baseline in the Sepsis-PBS group, while no significant difference was observed between baseline and day 13 in the β-NMN–treated group (Fig. S3B and C). Consistent with this functional preservation, transmission electron microscopy revealed that mitochondria in the gastrocnemius muscles of β-NMN–treated mice with sepsis exhibited a significant lower proportion of abnormal mitochondria compared with untreated septic mice. In untreated septic mice, abnormal mitochondria frequently displayed characteristic ultrastructural features, including loss of mitochondrial membrane continuity, disorganized cristae structure, and reduced matrix electron density (Fig. 4F). Collectively, these findings indicate that β-NMN supplementation attenuated

◀**Fig. 3**. Impaired respiration associated with *Sirt3* knockdown is partially rescued by *β*-NMN treatment in C2C12. (**A**) Immunoblot of mitochondrial fractions isolated from gastrocnemius muscle of control and sepsis mice at day 4 after cecal slurry injection, probed with anti–acetyl-lysine. Coomassie brilliant blue (CBB) staining was performed in parallel as a loading control. Arrowheads indicate bands excised for mass spectrometry analysis. (**B**) Top 10 candidate proteins identified using liquid chromatography- tandem mass spectroscopy (LC–MS/MS) from the differentially acetylated bands. (**C**) Experimental protocol for *Sirt3* knockdown in C2C12 myotubes. Myoblasts were transfected with *Sirt3* or scramble small interfering (siRNA) prior to differentiation, with repeated transfection at day 3. (**D**) Validation of *Sirt3* knockdown using qPCR, showing reduced *Sirt3* mRNA expression compared with a scramble control. (**E**) Validation of *Sirt3* knockdown using immunoblotting, showing reduced Sirt3 protein expression compared with scramble control. (**F**) Seahorse mitochondrial stress test of C2C12 myotubes (scramble vs *Sirt3* siRNA). *Sirt3* knockdown reduced basal respiration, maximal respiration, and ATP production. (**G**) Experimental protocol for Sirt3 knockdown in C2C12 myotubes. Myoblasts were transfected with Sirt3 or scramble small interfering (siRNA) prior to differentiation, with repeated transfection at day 3, and β-nicotinamide mononucleotide (β-NMN) was added at day 4 where indicated. (**H**) Intracellular NAD^+ concentrations in control, Sirt3-knockdown (DMEM), and Sirt3-knockdown cells treated with *β*-NMN. (**I**) Seahorse mitochondrial stress test with *β*-NMN treatment. *β*-NMN partially restored basal respiration and ATP production in *Sirt3* knockdown myotubes, whereas maximal respiration remained suppressed. Data are presented as mean ± SEM. Statistical analysis was performed using two-way ANOVA (with factors siRNA and treatment) followed by Bonferroni post hoc tests, or Welch's *t*-test for two-group comparisons. $*p < 0.05$, $**p < 0.01$, ns, not significant. Western blots in Panel (A) and (E) were cropped. For the full, uncropped Western blot, refer to Supplementary Information.

sepsis-induced muscle weakness, at least in part, in the context of improving mitochondrial morphology rather than by altering skeletal muscle mass.

Discussion

In this study, we demonstrated that young mice with sepsis exhibited persistent muscle weakness despite recovery of muscle mass. This dysfunction was associated with mitochondrial abnormalities and was ameliorated by administering *β*-NMN.

Our results in young mice showed body weight and skeletal muscle mass initially declined but recovered by day 14. In contrast, muscle strength remained impaired despite morphological recovery, and ultrastructural analysis revealed persistent mitochondrial abnormalities, including swelling and disruption of cristae. These results indicate that sepsis led to prolonged impairment of muscle contractility, even after apparent restoration of muscle mass. Previous studies in aged animal models have demonstrated that sepsis-induced muscle weakness can persist even after muscle mass recovery, with mitochondrial structural and functional abnormalities contributing to this dysfunction[8,10]. In addition, reports of clinical studies in ICU survivors of sepsis have revealed persistent skeletal muscle weakness, with reduced exercise capacity and impaired quality of life persisting for more than one year after discharge, supporting the findings of our study when contrasted with consistency of the sepsis model mouse with clinically tested conditions[7,23]. While sepsis can affect patients across all ages, advanced age is a major risk factor for ICU-AW, alongside prolonged immobilization, disease severity, and comorbidities[7]. Importantly, older patients with sepsis not only experience higher in-hospital mortality, but also present with worse long-term outcomes, including persistent functional decline, cognitive impairment, and increased dependence on long-term care[24,25]. We utilized young mice to establish a stable and reproducible model of sepsis and to minimize age-related confounders. This design enabled mechanistic analyses focused on sepsis per se, including longitudinal functional testing and mitochondrial readouts. Taken together, our findings extend these observations by demonstrating that even young mice with sepsis develop persistent muscle weakness accompanied by mitochondrial abnormalities despite recovery of muscle mass. This suggests that mitochondrial dysfunction is a fundamental and age-independent mechanism underlying post-sepsis muscle impairment in mice and underscores the potential clinical relevance of our model.

Our transcriptomic analysis using the gastrocnemius muscle in the acute phase of sepsis revealed significant enrichments of pathways related to sirtuin signaling, mitochondrial dysfunction, and oxidative phosphorylation, indicating that sepsis profoundly disrupted transcriptional programs governing mitochondrial homeostasis and energy metabolism by altering mitochondria-related molecules. qPCR validation confirmed that mitochondrial sirtuins, including *Sirt3, Sirt4*, and *Sirt5*, were downregulated, with *Sirt3* highlighted as a candidate regulator. Previous studies have shown that SIRT3, a major mitochondrial NAD^+-dependent deacetylase, maintains respiratory chain function by regulating protein acetylation, and that its downregulation under metabolic stress or sepsis contributes to hyperacetylation of mitochondrial proteins, reduced complex activity, and impaired ATP production[15,26]. While our data specifically highlighted SIRT3, it is noteworthy that other mitochondrial sirtuins, such as SIRT4 and SIRT5, also contribute to metabolic regulation under stress conditions. SIRT4 modulates lipid metabolism and ATP homeostasis in mitochondria[27], whereas SIRT5 modulates key metabolic pathways, including the tricarboxylic acid cycle (TCA), fatty acid oxidation, and reactive oxygen species detoxification through desuccinylase and demalonylase activity[28]. These sirtuins may also influence the pathophysiology of sepsis-induced mitochondrial dysfunction, although their precise roles remain to be elucidated. Given that global NAD^+ depletion can impair the activity of sirtuins, future studies should further clarify the roles of SIRT4 and SIRT5 in sepsis-induced metabolic dysfunction. Our findings indicate that sepsis suppresses multiple mitochondrial sirtuins, potentially involving not only SIRT3 but also SIRT4 and SIRT5. This suggests that mitochondrial dysfunction in sepsis-induced muscle impairment may result from a broad suppression of

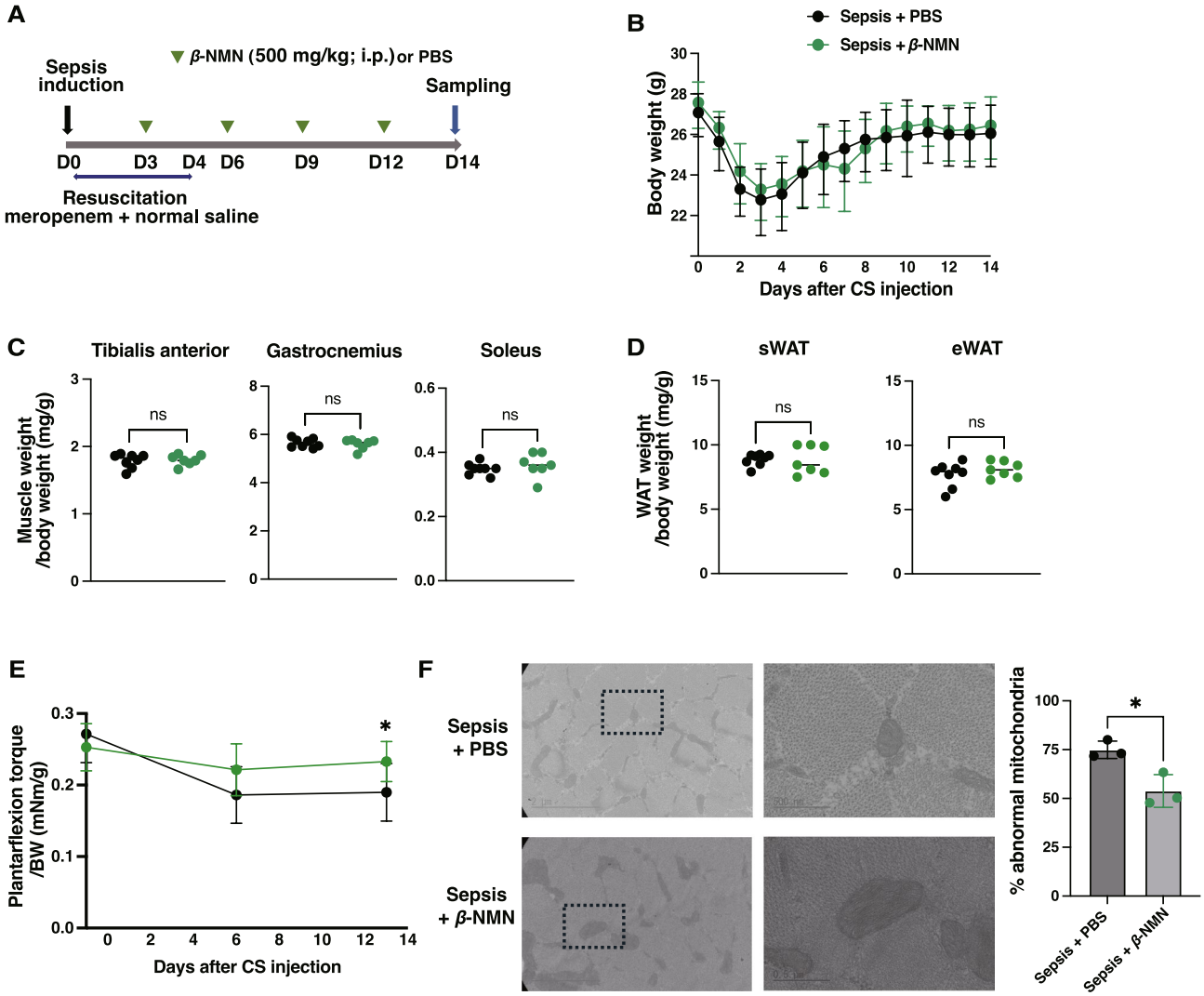

Fig. 4. β-NMN prevented functional decline in skeletal muscle after sepsis. (**A**) Experimental timeline of the cecal slurry (CS)–induced sepsis model with β-NMN treatment. Sepsis was induced on day 0 (D0), mice were resuscitated with meropenem and normal saline, andβ-nicotinamide mononucleotide (β-NMN; 500 mg/kg, intraperitoneal [i.p.]) or PBS was administered on D3, D6, D9, and D12. (**B**) Body-weight changes after cecal slurry injection in sepsis + PBS (n = 8) and sepsis + β-NMN (n = 7) groups (same mice followed up to D14). (**C**) Muscle weights of tibialis anterior, gastrocnemius, and soleus at D14. (**D**) Weights of subcutaneous and epididymal white adipose tissue (sWAT and eWAT, respectively) depots on D14. (**E**) Ratio of plantarflexor torque to body weight, measured at one day before sepsis induction (baseline), and on days 6 and 13 after sepsis induction in the same mice to assess functional recovery following sepsis. (**F**) Representative transmission electron microscopy images of gastrocnemius muscle mitochondria in sepsis + PBS and sepsis + β-NMN groups. The boxed areas in the left panels are shown at higher magnification in the right panels. Scale bars: 2 μm (left panels) and 500 nm (right panels). Data are mean ± SEM. Longitudinal data in Panel B (measured daily up to day 14) and data in Panel E (measured at three time points: days −1, 6, and 13) were analyzed using two-way repeated-measures ANOVA (factors: group and time) with Bonferroni post hoc tests. Single time point comparisons (**C** and **D**) were analyzed using unpaired Welch's *t*-tests. $^{*}p < 0.05$; ns, not significant.

mitochondrial deacetylation systems, highlighting mitochondrial sirtuins as potential therapeutic targets in ICU-AW.

In addition, our mass spectrometry analysis of lysine-acetylated bands from isolated mitochondria revealed several candidate proteins that may be targets of SIRT3, including components related to mitochondrial complex I. Although the specific targets remain to be determined, these findings raise the possibility that abnormal acetylation of complex I subunits may contribute to sepsis-induced mitochondrial dysfunction. Consistent with these findings, knockdown of *Sirt3* in C2C12 myotubes resulted in impaired mitochondrial respiration, as indicated by decreases in basal and maximal respiration, ATP production, and proton leakage. These results suggest that *Sirt3* is involved in the regulation of mitochondrial protein acetylation and respiratory function

in skeletal muscle. Previous studies have shown that SIRT3 regulates the acetylation status of mitochondrial respiratory chain proteins[15], including isocitrate dehydrogenase 2 to promote nicotinamide adenine dinucleotide phosphate production and antioxidant defense[29], succinate dehydrogenase to sustain the TCA cycle and electron transport chain activity[30], and superoxide dismutase 2 (SOD2) to reduce oxidative stress[31], and the complex I subunit NADH:ubiquinone oxidoreductase subunit A9 to maintain oxidative phosphorylation efficiency and ATP synthesis[15]. Building on these reports, our data suggest that mitochondrial protein hyperacetylation occurs alongside SIRT3 downregulation and may be involved in skeletal muscle mitochondrial dysfunction in sepsis.

The increased mitochondrial protein acetylation observed in septic muscle together with the impaired respiratory capacity seen in *Sirt3*-deficient C2C12 myotubes highlight not only the importance of mitochondrial regulation, but also the potential for nutritional strategies targeting NAD^+ metabolism. Traditional nutritional therapy in the ICU has primarily focused on supplying sufficient calories and protein to prevent catabolism and support recovery[32,33]. However, these conventional approaches have shown only partial benefit in preventing ICU-AW and do not adequately restore long-term muscle function[34,35]. Our findings highlight the importance of targeting mitochondrial quality and NAD^+ metabolism, rather than focusing solely on macronutrient provision. In this context, the administration of NAD^+ precursors such as β-NMN may represent a novel nutritional intervention that directly enhances mitochondrial bioenergetics and skeletal muscle function. Such molecularly targeted nutritional strategies could complement existing approaches and may ultimately lead to a paradigm shift in nutritional therapy for survivors of sepsis.

Consistent with the role of NAD^+ metabolism in SIRT3 activity, we found that acute-phase administration of β-NMN, a key NAD^+ precursor, preserved skeletal muscle strength and mitochondrial morphology in septic mice, despite no effect on body weight or muscle mass. These findings suggest that NAD^+ repletion may attenuate sepsis-induced mitochondrial damage and muscle dysfunction primarily through preservation of mitochondrial quality rather than modulation of muscle size. Previous studies have shown that NAD^+ levels decline markedly during sepsis and other inflammatory conditions[36], and supplementation with NAD^+ precursors such as β-NMN has been reported to restore mitochondrial function and improve outcomes in mouse models of cardiac injury[37,38]. Importantly, NAD^+ depletion is a reported hallmark of sepsis pathophysiology[36], which further supports the rationale for targeting NAD^+ metabolism as a therapeutic strategy. Our study extends these findings to skeletal muscle, showing that β-NMN supplementation is associated with preservation of mitochondrial structure and function, thereby mitigating ICU-AW–like symptoms. Taken together, these results highlight NAD^+ metabolism as a promising therapeutic target for sepsis-induced muscle impairment and suggest that nutritional interventions with β-NMN may complement conventional ICU therapy.

This study has several limitations. First, the therapeutic effect of β-NMN was not considered in aged septic mice. Second, our analyses were restricted to the acute and early recovery phases, and the long-term trajectory of muscle function after sepsis remains unknown. Third, while β-NMN administration better preserved muscle strength and preserved mitochondrial morphology, we did not directly measure NAD^+ levels, nor did we evaluate the potential contribution of anti-inflammatory effects; therefore, the precise mechanisms remain to be clarified. Fourth, body weight measurements during sepsis may be influenced by factors such as oedema and reduced food intake; however, neither oedema formation nor food intake was directly assessed in the present study. Fifth, the *Sirt3* knockdown experiments were performed *in vitro*, and *in vivo* validation is needed to establish causality. Finally, although transcriptomic and biochemical analyses suggested a role for SIRT3 in sepsis-induced mitochondrial dysfunction, we did not explore whether inflammatory signaling affects SIRT3 activity *in vivo*. Future studies should consider the impact of aging, assess long-term outcomes, and further elucidate both SIRT3-dependent and -independent mechanisms of potential NAD^+-boosting interventions such as β-NMN.

In summary, our study demonstrated that sepsis in young mice causes long-lasting impairment of skeletal muscle function despite recovery of muscle mass, accompanied by mitochondrial structural abnormalities and altered protein acetylation. Transcriptomic and biochemical analyses implicate SIRT3 as a potential key regulator of sepsis-induced mitochondrial dysfunction. Importantly, acute-phase administration of β-NMN better preserved muscle strength and mitochondrial morphology in the sepsis model, supporting the therapeutic potential of NAD^+-boosting interventions. These findings suggest that therapeutic approaches targeting mitochondrial quality and NAD^+ metabolism such as β-NMN treatment, may be promising strategies for mitigating post-sepsis muscle dysfunction and ICU-AW.

Materials and methods

Animals and husbandry

C57BL/6 J male mice were obtained from Jackson Laboratory Japan, Inc. (Yokohama, Japan). All mice were housed in a specific pathogen–free facility under climate-controlled conditions with a 12-h light/12-h dark cycle and were provided with water and a standard diet (MF; Oriental Yeast Co. Ltd., Tokyo, Japan) *ad libitum*. All animal experiments were approved by the Animal Experiment Committee of Ehime University (approval nos. 37A14-1 and 37A14-16) and conducted in accordance with the Ehime University Guidelines for Animal Experiments. All animal procedures and reporting complied with ARRIVE guidelines.

Preparation of cecal slurry and sepsis induction

A sepsis mouse model was established based on a previously reported method with slight modifications[16]. Briefly, 16-week-old male C57BL/6 J mice were used for the preparation of cecal slurry (CS). Mice were euthanized using ketamine (90 mg/kg) and xylazine (10 mg/kg) and the cecum were harvested. Cecal contents were collected and directly suspended in 10% glycerol in phosphate-buffered saline (PBS) at a ratio of 1.0 mL per 100 mg of contents. The suspension was filtered through nylon mesh sheets with sequentially smaller pore sizes (860, 380, 190, and 70 μm) which were cut to size and autoclaved before use. While stirring continuously with a magnetic stirrer, the CS was aliquoted into cryovials and stored at –80 °C until use. Sepsis was induced

in 11–13-week-old male C57BL/6 J mice, weighing 25–29 g, via a single intraperitoneal injection of CS at a dose corresponding to the minimum lethal dose, defined as the amount resulting in 100% mortality within 48 h in the absence of resuscitation. Mice were randomly assigned to experimental groups based on body weight. Control mice received an equal volume of 10% glycerol in PBS. At 12 h after CS injection, all mice were treated with meropenem (0.5 g/vial; NIPRO or Meiji Seika Pharma Co., Ltd., Tokyo, Japan) dissolved in 100 mL of sterile saline and administered intraperitoneally at a fixed volume of 300 µL per mouse twice daily (every 12 h) for 5 consecutive days. This dose corresponds to approximately 52–60 mg/kg for mice. In addition, mice were resuscitated using 700 µL of sterile saline administered subcutaneously twice daily (every 12 h). Body temperature and body weight were monitored regularly after sepsis induction. The meropenem and saline were pre-warmed to 37 °C before administration.

RNA-seq analysis

High-quality total RNA was extracted from gastrocnemius muscles collected from control mice (n = 5) and mice on day 4 after sepsis induction (n = 3) using RNeasy spin column kits (QIAGEN, Cat. No. 74106, Hilden, Germany), according to the manufacturer's protocol. RNA quality was verified using an Agilent 2100 Bioanalyzer (Agilent Technologies, Santa Clara, CA, USA). RNA sequencing was performed at the Kazusa DNA Research Institute (Chiba, Japan) using an Illumina NextSeq 500 platform with a read configuration of 75 base-pair single-end reads. One million reads were generated per sample. Data analysis was performed using CLC Genomics Workbench (version 23.0.2, Qiagen; https://digitalinsights.qiagen.com/) for read mapping and quantification. Differential expression analysis was performed using the Differential Expression for RNA-Seq tool implemented in QIAGEN CLC Genomics Workbench. Raw read counts were used for the analysis and normalized using the trimmed mean of M-values (TMM) method. Differential expression was assessed based on a negative binomial generalized linear model, and statistical significance was evaluated using the Wald test. P-values were adjusted for multiple testing using the Benjamini–Hochberg false discovery rate (FDR) method. Differentially expressed genes (DEGs) were defined as those with an absolute log2-fold change greater than 1 ($|\log2FC| > 1$) and an adjusted p-value (FDR) < 0.001. Pathway and functional enrichment analyses of DEGs were conducted using Ingenuity Pathway Analysis (IPA; content version 90,348,151, QIAGEN; https://digitalinsights.qiagen.com/).

RT-PCR

Total RNA was extracted from gastrocnemius muscles (control, n = 5; sepsis, n = 3) or C2C12 cells using Isogen (Nippon Gene Co., Ltd., Cat. No. 319–90,211, Tokyo, Japan) and RNeasy spin column kits (Qiagen, Cat. No. 74106, Germany). First-strand cDNA was synthesized from total RNA using PrimeScript RT Master Mix (Takara Bio, Inc.) and subjected to RT-PCR using TB Green Premix Ex Taq II (Takara Bio, Inc.) with Thermal Cycler Dice (Takara Bio, Inc.) according to the manufacturer's instructions. Relative gene expression levels were calculated using the $2^{-\Delta\Delta Ct}$ method and normalized to Rpl13a expression.

Histological analyses

Mice were anesthetized using a mixture of ketamine (90 mg/kg) and xylazine (10 mg/kg) and then euthanized by cervical dislocation. For immunofluorescence staining, harvested gastrocnemius muscles were rapidly frozen in liquid nitrogen–chilled isopentane. Unfixed cryosections of 10-µm thickness were prepared using a cryostat and air-dried at room temperature. Sections were blocked with Mouse on Mouse reagent (Vector Laboratories, Cat. No. MKB-2213-1, Newark, CA, USA) at room temperature for 60 min. Primary antibodies against myosin heavy chain type IIa (DSHB, Iowa City, IA, USA, Cat. No. SC-71, 1:100 dilution) and type IIb (DSHB, Cat. No. BF-F3, 1:100 dilution) diluted in 1% bovine serum albumin in PBS were applied with Laminin (Sigma-Aldrich, Cat. No. L9393, 1:500 dilution) and incubated at 37 ℃ for 45 min. After washing, sections were incubated with secondary antibodies, such as goat anti-mouse IgG1 Alexa Fluor 568 (Thermo Fisher Scientific, 1:1000 dilution), goat anti-mouse IgM Alexa Fluor 488 (Thermo Fisher Scientific, 1:1000 dilution), and goat anti-rabbit IgG Alexa Fluor 647 (Thermo Fisher Scientific, 1:1000 dilution) at 37 ℃ for 30 min. Following incubation and subsequent washes, images were acquired using a fluorescence microscope (Axio Observer 7; Zeiss, Oberkochen, Germany) and captured with ZEN imaging software (version 3.7; ZEISS; https://www.zeiss.com/). The CSA of each muscle fiber type was analyzed using image analysis software (n = 3 per group). To quantify the CSA, and minimum Feret diameter of the myofibers, captured images of entire cross-sections were analyzed using FIJI (Image J; version 2.16.0; https://imagej.net/software/fiji/). The myofiber area was identified using the laminin signals. The region of interest (ROI) was set within the laminin areas. The frequency of each muscle fiber type in the ROI was recorded using Trainable Weka Segmentation in FIJI after manual training[39]. Hematoxylin and eosin (H&E) staining was performed on lung and kidney tissues collected on day 4 after sepsis induction. Tissues were fixed in 4% paraformaldehyde, embedded in paraffin, sectioned at 5 µm thickness, and stained with hematoxylin and eosin according to standard procedures. Images were acquired using a light microscope (BX53; Olympus, Tokyo, Japan).

Measurement of serum IL-6 levels

Blood samples were collected by cardiac puncture at the time of sacrifice on day 4 after sepsis induction. Samples were centrifuged at 3000 × g for 10 min at 4 °C to obtain serum, which was frozen and stored at − 80 °C until analysis. Serum IL-6 concentrations were measured using a mouse IL-6 enzyme-linked immunosorbent assay (ELISA) kit according to the manufacturer's instructions (R&D Systems, Cat. No. M6000B-1, Minneapolis, MN, USA).

Muscle strength testing

Plantarflexion force of the ankle joint was measured using a muscle strength measurement system for mice (NGM-1, Bio Research Center Co., Ltd., Nagoya, Japan). Mice were anesthetized using a mixture of 0.3 mg/kg medetomidine, 4.0 mg/kg midazolam, and 5.0 mg/kg butorphanol. To prevent anesthesia-associated hypothermia, mice were placed on a thermostatically controlled heating pad set at 37 °C throughout the procedure and during the recovery period until full awakening. Electrical stimulation was applied to induce contraction of the plantar flexor muscles, and the force exerted by the hind paws on the footplate was detected via a load cell. Measurements were performed at three time points: one day before sepsis induction (baseline), and on days 6 and 13 after sepsis induction. For each time point, 10 consecutive measurements were conducted per mouse, and the average value was used for analysis (control, n = 4; sepsis, n = 6; sepsis + PBS, n = 8; sepsis + β-NMN, n = 7).

Transmission electron microscopy

After euthanasia performed under anesthesia induced by a mixture of ketamine (90 mg/kg) and xylazine (10 mg/kg), gastrocnemius muscles were collected (n = 3 per group). A small tissue mass was pre-fixed in 2% paraformaldehyde and 2% glutaraldehyde in 30 mM HEPES buffer (pH 7.4) at 4 °C for 16 h, and then post-fixed in 1% osmium tetroxide at 4 °C for 1.5 h. Samples were dehydrated in a graded ethanol series before being embedded in epoxy resin. Ultrathin 70-nm sections were prepared using an ultramicrotome (Ultracut R, Leica Microsystems) and mounted on grids. Sections were stained on dental wax supports with 4% uranyl acetate for 20 min in the dark, washed twice in 50% ethanol, and air-dried on filter paper. Sections were subsequently stained with 0.4% lead citrate for 10 min, washed twice in distilled water, and air-dried. Finally, carbon coating was performed using a vacuum evaporator (JEE-5B, JEOL Ltd., Tokyo, Japan) with the section-bearing side facing upward. Images were acquired using a transmission electron microscope (JEM-1230, JEOL Ltd.) at magnifications of 100,000 × and 3000 × to evaluate mitochondrial morphology. Mitochondria were classified as either normal or abnormal based on predefined morphological criteria, including cristae integrity, matrix density, and membrane continuity. Mitochondria exhibiting one or more abnormal features were classified as abnormal. For each sample, mitochondria were quantified in five randomly selected fields. The percentage of abnormal mitochondria was calculated for each sample, and data were averaged per sample for statistical analysis.

β-NMN treatment

β-nicotinamide mononucleotide (β-NMN; Cat. No. 44501000, Oriental Yeast Co., Ltd.) was diluted in sterile PBS for *in vivo* experiments or in DMEM for *in vitro* experiments. The prepared solutions were used immediately without storage. For *in vivo* experiments, mice were randomly assigned to treatment groups, and intraperitoneally injected with β-NMN at a dose of 500 mg/kg twice a week from days 3 to 14 after sepsis induction. The dose was selected based on previous studies demonstrating its efficacy in increasing tissue NAD^+ levels in mice, without apparent adverse effects[40]. Septic mice receiving an equal volume of PBS on the same schedule were used as the sepsis PBS group. A total of 15 septic mice were used for the β-NMN intervention experiment (sepsis + PBS, n = 8; sepsis + β-NMN, n = 7). For *in vitro* experiments, β-NMN was added to DMEM at a final concentration of 500 μM and incubated for 24 h. Control cells were treated with the same volume of vehicle (DMEM).

Isolation of mitochondria

Approximately 100 mg of gastrocnemius tissue was harvested and homogenized using a BioMasher disposable homogenizer (Nippi Inc., Tokyo, Japan) in 1 mL of ice-cold mitochondrial isolation buffer (250 mM sucrose, 5 mM Tris–HCl, 1 mM EDTA, 10 mM DTT, pH 7.4) supplemented with protease inhibitors. The homogenate was transferred to a microtube and centrifuged at 800 × g for 10 min at 4 °C. The supernatant (approximately 500 μL) was carefully transferred to a new tube and then centrifuged at 12,000 × g for 15 min at 4 °C to pellet the mitochondria[41]. The pellet was resuspended in approximately 500 μL of RIPA buffer (Nacalai Tesque, Cat. No. 16488-34) with protease inhibitor cocktail (Nacalai Tesque) for Western blotting.

Western blotting

The protein lysis was mixed with sodium dodecyl sulfate (SDS) sample buffer and boiled at 95 °C for 5 min. Samples were applied to 12.5% SuperSep Ace polyacrylamide gels (Wako, Cat. No. 196-14,981) and SDS–polyacrylamide gel electrophoresis was conducted for 60 min and transferred to PVDF membranes (Bio-Rad Laboratories, Cat. No. 1620177) using a mini transblot cell (Bio-Rad Laboratories, Cat. No. t 1703930JA). After transfer, membranes were blocked with 3% bovine serum albumin (BSA) and 0.2% skim milk in TBS containing Triton X-100 for 60 min at room temperature. Membranes were incubated with anti-acetyl lysine antibody (Cell Signaling Technology, Cat. No. 9441, 1:1000 dilution) overnight at 4 °C. After washing, the membranes were incubated with horseradish peroxidase-conjugated secondary antibodies for 60 min at room temperature. Immunoreactive signals were detected using Prime Western Blotting Detection Reagent (Cytiva, Cat. No. RPN2232, Marlborough, MA, USA) and visualized using the Amersham ImageQuant 800 imaging system (Cytiva).

Mass spectrometric analysis

The mitochondrial fractions were subjected to SDS-PAGE, and bands were excised from the gel and analyzed using LC–MS/MS. Briefly, extracted peptides were analyzed by ESI–MS/MS using a Q Exactive Orbitrap instrument (Thermo Fisher Scientific, Pittsburgh, PA, USA). MS spectra were recorded over a range of 350–1500 m/z, followed by data-dependent higher energy collisional dissociation (HCD) MS/MS spectra generated from the 10 highest intensity precursor ions.

For protein identification, spectra were processed using Proteome Discoverer version 2.5.0.400 (Thermo Fisher Scientific; https://www.thermofisher.com/) against Mascot algorithm. For database searches, mouse·.fasta built from the SwissProt (May 16, 2025) was used. The following parameters were used for the searches: tryptic cleavage, up to two missed cleavage sites, and tolerances of ± 10 ppm for precursor ions, and ± 0.5 Da for MS/MS fragment ions. Mascot searches were performed allowing optional methionine oxidation and fixed cysteine carbamidomethylation. Proteins that containinged peptides with Mascot Significance Threshold > 0.05 were selected.

Cell analysis

C2C12 cells (female, ATCC, CRL-1772) obtained from the American Type Culture Collection (ATCC, Manassas, VA, USA) were cultured in growth medium composed of high-glucose DMEM (Wako, Cat. No. 043-30,085, Japan) supplemented with 10% fetal bovine serum, 1% antibiotic mixture, and Amphotericin B (Gibco, Cat. No. 15290-018, Waltham, MA, USA). To induce differentiation of myotubes, the medium was switched to a differentiation medium (DMEM containing 2% horse serum) when cells reached 70–80% confluence. At the time of differentiation induction, cells were transfected using siRNA targeting *Sirt3* (ON-TARGETplus SMARTpool siRNA; Dharmacon [Horizon Discovery], Lafayette, CO, USA) using Lipofectamine RNAiMAX (Thermo Fisher Scientific) according to the manufacturer's protocol. The final siRNA concentration was 10 nM for assays. Cells were at 70–80% confluence at the time of transfection. Transfection was repeated every other day during the differentiation period to maintain knockdown efficiency. A non-targeting siRNA (Dharmacon) was used as a control. Cells were collected on day 6 after differentiation for subsequent analyses.

Extracellular flux analysis of mitochondria function

Extracellular flux was assessed using a Seahorse XFp Analyzer (Agilent Technologies) as previously described[42]. Prior to starting the assay, C2C12 cells were seeded at a density of 1.2×10^3 cells/well in Seahorse XFp miniplates (8 well) and differentiated into myotubes and subjected to knockdown of *Sirt3* using siRNA. For oxygen consumption rate (OCR) analysis, cells were cultured for 60 min in DMEM, supplemented with 25 mM glucose, 1 mM pyruvate, and 2 mM glutamine (Seahorse Bioscience, pH 7.4 ± 0.1) and equilibrated at 37 °C in a CO_2-free atmosphere. After three basal measurements, 1 µM oligomycin, 2.0 µM carbonyl cyanide 4-(trifluoromethoxy) phenylhydrazone and 0.5 µM antimycin A/rotenone were sequentially injected into the plate. For analysis of the extracellular acidification rate, cells were cultured for 60 min in DMEM supplemented with 2 mM glutamine and equilibrated at 37 °C in a CO_2-free atmosphere. After three basal measurements, 10 mM glucose and 1 µM oligomycin were sequentially injected as described for OCR analysis. Data were analyzed using Wave software (version 2.6.4.24; Agilent Technologies; https://www.agilent.com/).

Intracellular NAD⁺ measurement

Intracellular NAD^+ levels were determined using an NAD/NADH Assay Kit-WST (N509; Dojindo Laboratories, Kumamoto, Japan). Prior to the assay, C2C12 cells were seeded at a density of 2×10^5 cells /well in 6-well plates. Then, cells were differentiated into myotubes and subjected to knockdown of *Sirt3* using siRNA. After washing with PBS, cell extracts were prepared using the extraction buffer provided with the kit. The extracts were centrifuged at 12,000 × g for 5 min, and the resulting supernatants were ultrafiltered using a 10-kDa molecular weight cut-off filter. For selective measurement of NADH, aliquots of the filtered samples were heat-treated at 60 °C according to the manufacturer's protocol. Subsequently, samples were subjected to an enzymatic reaction at 37 °C for 1 h, and absorbance at 450 nm was measured using a Multiskan SkyHigh microplate reader (Thermo Fisher Scientific). Total NAD (NAD^+ + NADH) and NADH levels were measured according to the manufacturer's protocol, and intracellular NAD^+ levels were calculated accordingly.

Statistics

All statistical analyses were performed using GraphPad Prism version 10.5 (GraphPad Software, San Diego, CA, USA; https://www.graphpad.com/scientific-software/prism/). Data are presented as mean ± standard error of the mean (SEM). Differences between groups were evaluated using unpaired two-tailed Welch's *t*-test. For comparisons among multiple groups, one-way or two-way analysis of variance (ANOVA) followed by Tukey's post hoc test was applied when all pairwise group comparisons were required, while the Šidák correction was used for selected pairwise comparisons to control the family-wise error rate. A p-value < 0.05 was considered statistically significant.

Data availability

The RNA-seq data have been deposited in the Gene Expression Omnibus database under the accession code GSE310375 (https://www.ncbi.nlm.nih.gov/geo/query/acc.cgi?acc=GSE310375). The mass spectrometry proteomics data have been deposited to the ProteomeXchange Consortium via the PRIDE partner repository with the dataset identifier PXD072078 (https://www.ebi.ac.uk/pride/archive/projects/PXD072078). All other data supporting the findings of this study are available within the article, its Supplementary information files, and from the corresponding author upon reasonable request.

Received: 9 October 2025; Accepted: 2 March 2026
Published online: 13 March 2026

References

1. Singer, M. et al. The third international consensus definitions for sepsis and septic shock (Sepsis-3). *JAMA* **315**, 801–810 (2016).

2. Needham, D. M. et al. Improving long-term outcomes after discharge from intensive care unit: Report from a stakeholders' conference. *Crit Care Med* **40**, 502–509 (2012).
3. Hermans, G. & Van den Berghe, G. Clinical review: Intensive care unit acquired weakness. *Crit. Care* **19**, 274 (2015).
4. Stevens, R. D. et al. Neuromuscular dysfunction acquired in critical illness: a systematic review. *Intensive Care Med* **33**, 1876–1891 (2007).
5. Chen, X., Lei, X., Xu, X., Zhou, Y. & Huang, M. Intensive care unit-acquired weakness in patients with extracorporeal membrane oxygenation support: Frequency and clinical characteristics. *Front. Med.* **9**, 792201 (2022).
6. Van Aerde, N. et al. Intensive care unit acquired muscle weakness in COVID-19 patients. *Intensive Care Med* **46**, 2083–2085 (2020).
7. Iwashyna, T. J., Ely, E. W., Smith, D. M. & Langa, K. M. Long-term cognitive impairment and functional disability among survivors of severe sepsis. *JAMA* **304**, 1787–1794 (2010).
8. Owen, A. M. et al. Chronic muscle weakness and mitochondrial dysfunction in the absence of sustained atrophy in a preclinical sepsis model. *Elife* https://doi.org/10.7554/eLife.49920 (2019).
9. Akama, Y. et al. Roles of programmed death-1 and muscle innate lymphoid cell-derived interleukin 13 in sepsis-induced intensive care unit-acquired weakness. *J. Cachexia Sarcopenia Muscle* **15**, 1999–2012 (2024).
10. Kingren, M. S. et al. Post-sepsis chronic muscle weakness can be prevented by pharmacological protection of mitochondria. *Mol. Med.* **30**, 221 (2024).
11. van Zanten, A. R. H., De Waele, E. & Wischmeyer, P. E. Nutrition therapy and critical illness: Practical guidance for the ICU, post-ICU, and long-term convalescence phases. *Crit. Care* **23**, 368 (2019).
12. Singer, P. et al. ESPEN practical and partially revised guideline: Clinical nutrition in the intensive care unit. *Clin. Nutr.* **42**, 1671–1689 (2023).
13. Hermans, G. et al. Effect of tolerating macronutrient deficit on the development of intensive-care unit acquired weakness: A subanalysis of the EPaNIC trial. *Lancet Respir. Med.* **1**, 621–629 (2013).
14. Zhang, L. et al. Early mobilization of critically ill patients in the intensive care unit: A systematic review and meta-analysis. *PLoS ONE* **14**, e0223185 (2019).
15. Ahn, B. H. et al. A role for the mitochondrial deacetylase Sirt3 in regulating energy homeostasis. *Proc. Natl. Acad. Sci. U. S. A.* **105**, 14447–14452 (2008).
16. Steele, A. M., Starr, M. E. & Saito, H. Late therapeutic intervention with antibiotics and fluid resuscitation allows for a prolonged disease course with high survival in a severe murine model of sepsis. *Shock* **47**, 726–734 (2017).
17. Rocheteau, P. et al. Sepsis induces long-term metabolic and mitochondrial muscle stem cell dysfunction amenable by mesenchymal stem cell therapy. *Nat Commun* **6**, 10145 (2015).
18. Pierre, A. et al. Muscle weakness after critical illness: Unravelling biological mechanisms and clinical hurdles. *Crit. Care* **29**, 248 (2025).
19. Imai, S., Armstrong, C. M., Kaeberlein, M. & Guarente, L. Transcriptional silencing and longevity protein Sir2 is an NAD-dependent histone deacetylase. *Nature* **403**, 795–800 (2000).
20. Imai, S. & Guarente, L. NAD+ and sirtuins in aging and disease. *Trends Cell Biol.* **24**, 464–471 (2014).
21. Lombard, D. B. et al. Mammalian Sir2 homolog SIRT3 regulates global mitochondrial lysine acetylation. *Mol. Cell Biol.* **27**, 8807–8814 (2007).
22. Verdin, E., Hirschey, M. D., Finley, L. W. & Haigis, M. C. Sirtuin regulation of mitochondria: Energy production, apoptosis, and signaling. *Trends Biochem. Sci.* **35**, 669–675 (2010).
23. Yende, S. et al. Long-term quality of life among survivors of severe sepsis: Analyses of two international trials. *Crit. Care Med.* **44**, 1461–1467 (2016).
24. Ge, S. et al. Post-discharge functional outcomes in older patients with sepsis. *Crit. Care.* **28**, 281 (2024).
25. Ibarz, M., Haas, L. E. M., Ceccato, A. & Artigas, A. The critically ill older patient with sepsis: A narrative review. *Ann. Intensive Care.* **14**, 6 (2024).
26. Zhang, Q., Siyuan, Z., Xing, C. & Ruxiu, L. SIRT3 regulates mitochondrial function: A promising star target for cardiovascular disease therapy. *Biomed. Pharmacother.* **170**, 116004 (2024).
27. Han, Y., Zhou, S., Coetzee, S. & Chen, A. SIRT4 and its roles in energy and redox metabolism in health, disease and during exercise. *Front. Physiol.* **10**, 1006 (2019).
28. Heinonen, T., Ciarlo, E., Le Roy, D. & Roger, T. Impact of the dual deletion of the mitochondrial sirtuins SIRT3 and SIRT5 on anti-microbial host defenses. *Front. Immunol.* **10**, 2341 (2019).
29. Someya, S. et al. Sirt3 mediates reduction of oxidative damage and prevention of age-related hearing loss under caloric restriction. *Cell* **143**, 802–812 (2010).
30. Cimen, H. et al. Regulation of succinate dehydrogenase activity by SIRT3 in mammalian mitochondria. *Biochemistry* **49**, 304–311 (2010).
31. Qiu, X., Brown, K., Hirschey, M. D., Verdin, E. & Chen, D. Calorie restriction reduces oxidative stress by SIRT3-mediated SOD2 activation. *Cell Metab.* **12**, 662–667 (2010).
32. Singer, P. et al. ESPEN guideline on clinical nutrition in the intensive care unit. *Clin. Nutr.* **38**, 48–79 (2019).
33. de Man, A. M. E., Gunst, J. & Reintam Blaser, A. Nutrition in the intensive care unit: From the acute phase to beyond. *Intensive Care Med.* **50**, 1035–1048 (2024).
34. Zhou, W., Shi, B., Fan, Y. & Zhu, J. Effect of early activity combined with early nutrition on acquired weakness in ICU patients. *Medicine* **99**, e21282 (2020).
35. Chapple, L. S., Parry, S. M. & Schaller, S. J. Attenuating muscle mass loss in critical illness: The role of nutrition and exercise. *Curr. Osteoporos. Rep.* **20**, 290–308 (2022).
36. Cao, T. et al. Nicotinamide mononucleotide as a therapeutic agent to alleviate multi-organ failure in sepsis. *J. Transl. Med.* **21**, 883 (2023).
37. Yamamoto, T. et al. Nicotinamide mononucleotide, an intermediate of NAD+ synthesis, protects the heart from ischemia and reperfusion. *PLoS ONE* **9**, e98972 (2014).
38. Ni, R. et al. Nicotinamide mononucleotide protects septic hearts in mice via preventing cyclophilin F modification and lysosomal dysfunction. *Acta Pharmacol. Sin.* **46**, 976–988 (2025).
39. Sakai, H. et al. The androgen receptor in mesenchymal progenitors regulates skeletal muscle mass via Igf1 expression in male mice. *Proc. Natl. Acad. Sci. U. S. A.* **121**, e2407768121 (2024).
40. Yoshino, J., Baur, J. A. & Imai, S. I. NAD(+) intermediates: The biology and therapeutic potential of NMN and NR. *Cell Metab.* **27**, 513–528 (2018).
41. Lampl, T., Crum, J. A., Davis, T. A., Milligan, C. & Del Gaizo Moore, V. Isolation and functional analysis of mitochondria from cultured cells and mouse tissue. *J Vis Exp* **97**, 52076 (2015).
42. Saeki, N. & Imai, Y. Reprogramming of synovial macrophage metabolism by synovial fibroblasts under inflammatory conditions. *Cell Commun. Signal.* **18**, 188 (2020).

Acknowledgements

We gratefully thank the members of the Advanced Research Support Center (ADRES), especially Dr. Takahiro Fukazawa, and the Division of Integrative Pathophysiology, Proteo-Science Center (PROS), Ehime University,

for their technical assistance and helpful support. We also appreciate the members of the Department of Emergency and Critical Care Medicine, Ehime University, for their valuable clinical insights and constructive discussions. We are especially grateful to Dr. Hiroshi Saito at the University of Kentucky for his generous guidance on the cecal slurry model.

Author contributions

Mari Saida (conceptualization, methodology, formal analysis, investigation, data curation, and writing—original draft and visualization), Noritaka Saeki (methodology, formal analysis, and writing—review and editing), Hiroshi Sakai (methodology, funding acquisition, and writing—review and editing), Jun Iwanami (resources, methodology, and writing—review and editing), Atsushi Yokoyama (resources, formal analysis, and writing—review and editing), Shun Sawatsubashi (resources, formal analysis, and writing—review and editing), Motoi Kanagawa (resources, methodology, and writing—review and editing), Norio Sato (conceptualization, supervision, funding acquisition, and writing—review and editing) and Yuuki Imai (conceptualization, methodology, resources, funding acquisition, project administration, supervision, and writing—review and editing). All authors reviewed and approved the final version of the submitted manuscript.

Funding

This work was supported by the Japan Society for the Promotion of Science (JSPS) KAKENHI (Grant Number JP23K08427).

Declarations

Competing interests

The authors declare no competing interests.

Additional information

Supplementary Information The online version contains supplementary material available at https://doi.org/10.1038/s41598-026-43172-w.

Correspondence and requests for materials should be addressed to Y.I.